

ODE_t (ODE_l): Shortcutting the Time and Length in Diffusion and Flow Models for Faster Sampling

Denis Gudovskiy* Wenzhao Zheng Tomoyuki Okuno Yohei Nakata Kurt Keutzer
Panasonic AI Lab UC Berkeley Panasonic Corp Panasonic Corp UC Berkeley

Abstract

Recently, continuous normalizing flows (CNFs) and diffusion models (DMs) have been studied using the unified theoretical framework. Although such models can generate high-quality data points from a noise distribution, the sampling demands multiple iterations to solve an ordinary differential equation (ODE) with high computational complexity. Most existing methods focus on reducing the number of time steps during the sampling process to improve efficiency. In this work, we explore a complementary direction in which the quality-complexity tradeoff can be dynamically controlled in terms of time steps and in the length of the neural network. We achieve this by rewiring the blocks in the transformer-based architecture to solve an inner discretized ODE w.r.t. its length. Then, we employ time- and length-wise consistency terms during flow matching training, and as a result, the sampling can be performed with an arbitrary number of time steps and transformer blocks. Unlike others, our ODE_t (ODE_l) approach is solver-agnostic in time dimension and decreases both latency and memory usage. Compared to the previous state of the art, image generation experiments on CelebA-HQ and ImageNet show a latency reduction of up to $3\times$ in the most efficient sampling mode, and a FID score improvement of up to 3.5 points for high-quality sampling. We release our code and weights with fully reproducible experiments².

1 Introduction

Recent flow matching (FM) for continuous normalizing flows (CNFs) [1–3] and previously explored diffusion models (DMs) [4–6] have been successful in modeling various data domains including images [7], videos [8], language [9], proteins [10], molecules [11], multimodal data [12], etc.

Tong et al. [14] have generalized the training phase in such models with the conditional FM (CFM) framework in Table 1 using the simulation-free regression objective. In addition, Song et al. [15] showed that the stochastic differential equation (SDE) to sample from the DM can be converted to a probability flow ordinary differential equation (ODE) that further unifies two types of generative models. Despite simplified training, CNFs and DMs have the major bottleneck in the sampling process where the ODE needs to be solved with a large number of function evaluations (NFE).

To improve efficiency, most existing methods focus on the minimization of NFE and propose various forms of knowledge distillation to decrease the number of ODE integration steps when sampling data from the noise distribution [16]. Dieleman [17] argues that, although practitioners could benefit from NFE reduction methods, *there is no free lunch and these methods are inherently limited by the quality-complexity tradeoff*. At the same time, a recent class of such methods e.g., shortcut models in Frans et al. [13] have provided the important property to dynamically control this tradeoff and to minimize the drop in sampling quality while maintaining a low NFE budget.

*Corresponding author: denis.gudovskiy@us.panasonic.com

²Our code and checkpoints are available at github.com/gudovskiy/odelt

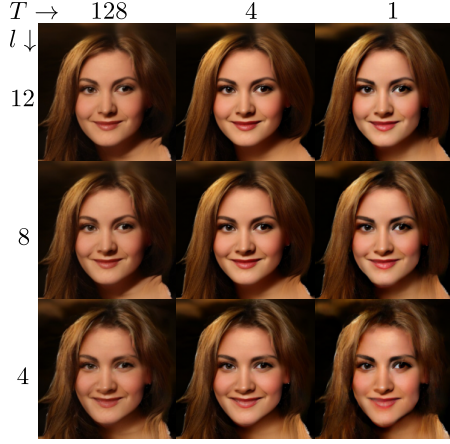


Figure 1: **ODE_{T|l,d}(ODE_l) sampling.** Time-wise shortcuts (SM) [13] (columns) alter the image style, our length-wise shortcuts (rows) preserve the style and iteratively compress the image details.

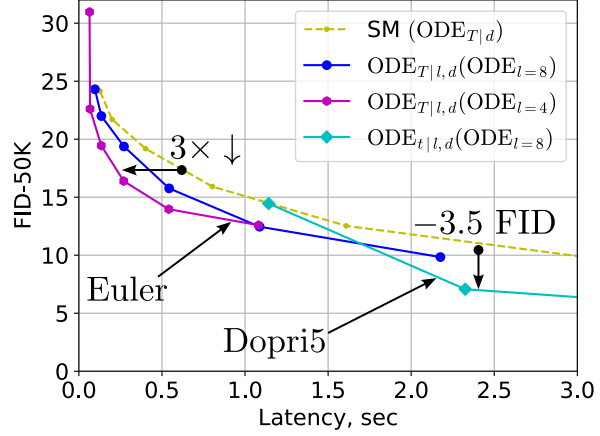


Figure 2: **FID vs. latency.** Our approach scales favorably when compared to SM [13]: it achieves up to 3× reduction in latency with Euler solver in compute-optimized mode, and provides up to 3.5 lower FID score with adaptive-step solver for high-quality sampling.

In this paper, we propose a complementary approach to reduce test-time computational complexity in CNFs and DMs. In addition to minimizing solely the NFE, we are motivated to modify the time-dependent neural network that approximates the target vector field. In particular, we consider an architecture that consists of a sequence of blocks e.g., the transformer-based DiT [18], where the number of active blocks can be dynamically changed. Then, the quality-complexity tradeoff also depends on the selected neural network length and scales better than the [13] as in Figures 1-2. Our objective can be achieved with minor architectural modifications and low computational overhead.

Our *ODE within ODE approach*, dubbed ODE_t (ODE_l), is sketched in Fig. 3. Unlike conventional architectures that treat the neural network $v_{\theta}(t, x_t)$ as a monolithic function, we consider it as a compositional function. When implemented as a sequence of blocks, it can solve an *inner discrete ODE* w.r.t. the sequence length. In particular, we condition the modeled vector field on the length l that defines the number of active blocks to produce a length-dependent inner ODE solution $v_{\theta}(l, t, x_t)$. Then, it is used for the *outer ODE* integration w.r.t. the time variable. For example, our neural network has the original full length when $l = L$. On the other hand, our method reduces the computational complexity with $l < L$ at the expense of sampling quality. Unlike NFE-only optimization, our method has the following advantages: a) the outer ODE is solver-agnostic, b) not only latency but also the memory overhead is proportional to the sequence length, and c) it supports sampling with dynamically selected time- and length-wise model shortcuts. Our main contributions are summarized as follows:

- Our ODE_t (ODE_l) generalizes shortcut models to the length dimension in CNFs and DMs.
- It is uniquely solver-agnostic in ODE_t and reduces latency and memory usage for ODE_l.
- Experiments show state-of-the-art results in the quality-complexity tradeoff scaling.

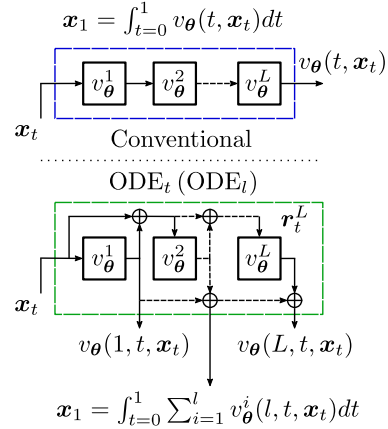


Figure 3: The conventional approach (top) models the interpolated vector field $u_t(x|z)$ by an expressive but monolithic neural network $v_{\theta}(t, x_t)$. This limits practitioners to adjust the quality-complexity tradeoff only in the integral’s time dimension. Our ODE_t (ODE_l) approach (bottom) considers the neural network as the inner ODE_l and allows to select the number of active blocks and, hence, reduce latency and memory usage during sampling.

2 Related work

In this section, we provide an overview of key concepts that have been used to advance efficiency in a class of generative models i.e. the CNFs and DMs. Then, we introduce up-to-date NFE minimization related work and present a broader context with developments in architecture-level optimizations.

Knowledge distillation. Knowledge distillation for discriminative models has been pioneered by Hinton et al. [19], who showed that a larger "teacher" network knowledge can be transferred to a smaller "student" one by mimicking the logit outputs without a substantial drop in speech and image recognition accuracy. An extension of this approach for generative CNFs and DMs has been realized by distilling such models w.r.t. the discretized time. With this approach, only a single time step [20] or a few steps [21, 22] of the student can be enough to mimic the teacher's ODE solution with reasonable precision. From the most recent literature survey [16], we highlight SlimFlow [23] with an explicit objective to distill to a smaller student network. Unlike SlimFlow, our ODE_t (ODE_l) architecture modifications lead to a number of sub-networks after the end-to-end training, where these sub-networks can also be considered as a special type of implicit student networks.

Consistency and rectified flows. Song et al. [24] propose a novel type of distillation where an explicit separate student network is not required, and a single-step model can be trained end-to-end from scratch. During consistency training, the neural network is constrained to be *self-consistent* i.e. points on the same ODE sampling trajectory map to the origin. Later, consistency models have been improved [25], simplified [26] and extended to the latent space [27].

Consistency is also related to the flow matching framework [1, 2] with straight paths e.g., rectified flows [28]. Compared to diffusion models, rectified flows can achieve higher sampling quality with fewer integration steps. This has been explored in Reflow [3] with the NFE minimization procedure. Frans et al. [13] propose to employ both self-consistency and straight trajectories, where the shortcuts in the rectified flow provide dynamic selection of \log_2 discrete sampling steps with lower quality overhead. Our method is complementary to NFE-only optimization methods, and results in better quality-complexity scaling when combined with time-wise shortcut models [13].

Efficient architectures. Architecture-level optimizations are typically explored separately from ODE acceleration. At the same time, minimization of the NFE is directly related to the complexity of the underlying neural network architectures. Earlier research has been proposed for discriminative models, including the concept of conditional computations [29] and its realizations in architectures that can dynamically drop [30] or skip [31] blocks in neural networks. Similarly, early exit strategies have been proposed for transformers [32] and more recently for DMs [33]. Moreover, Zhao et al. [34] propose dynamic diffusion transformers for the DiT architecture [18] with dynamic tokens in time and spatial dimensions during generation. Similarly, You et al. [35] introduce the dynamic architecture for DMs with efficient token-level routing mechanism.

Alternative architectures. Although our method incorporates vanilla DiT blocks with elements of dynamic conditional computation, it is analytically related to other types of architectures, as shown in Section 4. In this line of research, recent fixed point diffusion models [36] are derived from deep equilibrium models (DEQs) [37] where each layer has infinite depth. In contrast to DEQ models, we consider each DiT block as an ODE step for the fixed-step Euler solver rather than the implicit DEQ layers with non-ODE solvers [38]. Therefore, we rely on an ODE-centric architecture that has also been explored in various multi-step ResNet-type architectures for classifiers [39, 40], DMs [41], neural flows [42], neural residual DMs [43] and PDE-Nets [44]. Meanwhile, we propose our ODE_t (ODE_l) with the main motivation to advance efficiency by dynamically adjusting the compute in terms of time steps and active neural network layers when sampling from CNFs and DMs.

3 Preliminaries

Continuous normalizing flows. Our notation follows [1, 14]. There are a pair of data distributions $q(x_0)$ and $q(x_1)$ over \mathbb{R}^D with densities $p(x_0)$ and $p(x_1)$, respectively. Typically, $p_0 = p(x_0)$ represents a known prior distribution e.g., Gaussian. The task is to sample $x_1 \sim q(x_1)$ with unknown data density $p_1 = p(x_1)$ and only access to an empirical $\hat{q}(x_1)$.

Then, there are a *probability density path* $p : [0, 1] \times \mathbb{R}^D \rightarrow \mathbb{R}_{>0}$, which is a time-dependent probability density function $p_t(x)$ with $t \in [0, 1]$ such that $\int p_t(x) dx = 1$, and a time-dependent

Table 1: Generalization of diffusion and flow matching models by Tong et al. [14].

Probability Path	$q(\mathbf{z})$	$\mu_t(\mathbf{z})$	σ_t
Var. Exploding DM [5]	$q(\mathbf{x}_1)$	\mathbf{x}_1	$\frac{\sigma_{1-t}}{\sqrt{1-\alpha_{1-t}^2}}$
Var. Preserving DM [6]	$q(\mathbf{x}_1)$	$\alpha_{1-t}\mathbf{x}_1$	$\sqrt{1-\alpha_{1-t}^2}$
Flow matching (FM) [1]	$q(\mathbf{x}_1)$	$t\mathbf{x}_1$	$t\sigma - t + 1$
Rectified FM (RFM) [3]	$q(\mathbf{x}_0)q(\mathbf{x}_1)$	$t\mathbf{x}_1 + (1-t)\mathbf{x}_0$	0
Independent CFM [14]	$q(\mathbf{x}_0)q(\mathbf{x}_1)$	$t\mathbf{x}_1 + (1-t)\mathbf{x}_0$	σ
Var. Preserving. FM [2]	$q(\mathbf{x}_0)q(\mathbf{x}_1)$	$\cos(\pi t/2)\mathbf{x}_0 + \sin(\pi t/2)\mathbf{x}_1$	0

Lipschitz-smooth *vector field* $u : [0, 1] \times \mathbb{R}^D \rightarrow \mathbb{R}^D$. The vector field u_t is used to construct a time-dependent diffeomorphism i.e., the CNF $\phi : [0, 1] \times \mathbb{R}^D \rightarrow \mathbb{R}^D$ that is defined via the ODE as

$$d\phi_t(\mathbf{x})/dt = u_t(\phi_t(\mathbf{x})) \text{ and } \phi_0(\mathbf{x}) = \mathbf{x}_0, \quad (1)$$

where $\phi_t(\mathbf{x})$ is the ODE solution with $\phi_0(\mathbf{x})$ initial condition that transports \mathbf{x} from time 0 to time t .

On the other hand, ϕ_t induces a push-forward $p_t = [\phi_t]_{\#}(p_0)$ that transports the density p_0 from time 0 to time t . The time-dependent density p_t is characterized by the *continuity equation* written by

$$\partial p_t(\mathbf{x})/\partial t = -\text{div}(p_t(\mathbf{x})u_t(\phi_t(\mathbf{x}))) = -\text{div}(f_t(\mathbf{x})), \quad (2)$$

where the divergence operator, div , is defined as the sum of derivatives of $f_t(\mathbf{x}) \in \mathbb{R}^D$ w.r.t. all elements x_d or, simply, the Jacobian matrix trace: $\text{div}(f(\mathbf{x})) = \sum_{d=1}^D \partial f_d(\mathbf{x})/\partial x_d = \text{Tr}(\mathbf{J})$.

The vector field $u_t(\phi_t(\mathbf{x}))$ is often modeled without $\phi_t(\mathbf{x})$ invertability property by an arbitrary neural network $v_{\theta}(t, \mathbf{x}_t)$ with the learnable weight vector θ . Then, the continuity equation in (2) for (1) neural ODE can be written using the instantaneous change of variables [45] and trained by maximizing the likelihood (MLE) objective as

$$\arg \max_{\theta} \mathcal{L}_{\text{MLE}} := \log p_0 - \int_1^0 \text{Tr}(\partial v_{\theta}(t, \mathbf{x}_t)/\partial \mathbf{x}_t^T) dt, \quad (3)$$

where $\mathbf{x}_1 \sim \hat{q}(\mathbf{x}_1)$ and $\log p_0$ is evaluated using known prior e.g., the Gaussian noise $\mathbf{x}_0 \sim \mathcal{N}(\mathbf{0}, \mathbf{I})$.

DM and flow matching training. CNF training using the MLE objective (3) with integration is computationally expensive [46, 47]. The FM framework [1] proposes an alternative objective that regresses $v_{\theta}(t, \mathbf{x}_t)$ to u_t by conditioning the latter by a vector $\mathbf{z} = \mathbf{x}_1$. This has been extended by the conditional FM (CFM) framework [14] where $u_t(\mathbf{x}|\mathbf{z})$ and $p_t(\mathbf{x}|\mathbf{z})$ are conditioned on a more general $\mathbf{z} \sim q(\mathbf{z})$. Then, the Gaussian conditional probability path has a unique target conditional vector field that can be expressed by

$$p_t(\mathbf{x}|\mathbf{z}) = \mathcal{N}(\mathbf{x} | \mu_t(\mathbf{z}), \sigma_t(\mathbf{z})^2 \mathbf{I}) \implies u_t(\mathbf{x}|\mathbf{z}) = (\mathbf{x} - \mu_t(\mathbf{z}))\sigma_t'(\mathbf{z})/\sigma_t(\mathbf{z}) + \mu_t'(\mathbf{z}), \quad (4)$$

where the mean $\mu_t(\mathbf{z})$ and the standard deviation $\sigma_t(\mathbf{z})$ functions parameterize the path $p_t(\mathbf{x}|\mathbf{z})$.

Finally, the CFM regression objective for simulation-free CNF training using (4) result is

$$\arg \min_{\theta} \mathcal{L}_{\text{CFM}} := \mathbb{E}_{t \sim \mathcal{U}(0,1), \mathbf{x}_t \sim p_t(\mathbf{x}|\mathbf{z}), \mathbf{x} \sim \mathcal{N}(\mathbf{0}, \mathbf{I}), \mathbf{z} \sim q(\mathbf{z})} \|v_{\theta}(t, \mathbf{x}_t) - u_t(\mathbf{x}|\mathbf{z})\|^2. \quad (5)$$

The CFM training framework in (5) can be generalized to diffusion models by choosing appropriate $\mu_t(\mathbf{z})$ and $\sigma_t(\mathbf{z})$ as shown in Table 1. Meanwhile, the ODE perspective (1) for DMs [15] is particularly useful for the faster deterministic sampling that has been discussed in [48, 1].

4 Proposed method

Compositionality as the inner ODE. Although (5) avoids integration in (3) during training, the sampling process still requires to solve the ODE in (1) with either adaptive-step solver or a solver with discretization and fixed time steps. In general case, the sampling can be written as

$$d\phi_t(\mathbf{x})/dt = u_t(\phi_t(\mathbf{x})) \implies \mathbf{x}_1 = \int_0^1 v_{\theta}(t, \mathbf{x}_t) dt. \quad (6)$$

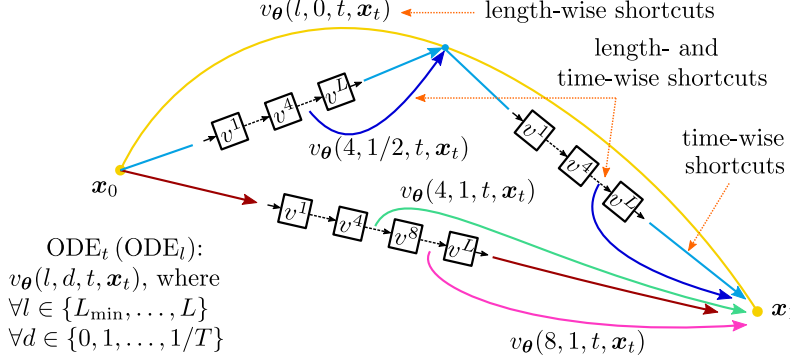


Figure 4: **Overview of ODE_t (ODE_l) shortcuts.** Our approach models the target vector field using the configurable $v_\theta(l, d, t, \mathbf{x}_t)$ neural network. The length hyperparameter l defines the number of active blocks within the architecture i.e. length-wise shortcuts. The time-wise shortcuts are adjusted by the hyperparameter d as proposed by Frans et al. [13]. Then, several cases can be highlighted: a) $v_\theta(L, 0, t, \mathbf{x}_t)$ is equivalent to the conventional CFM/DM processing, b) $v_\theta(L, d, t, \mathbf{x}_t)$ is identical to the time-wise only shortcuts (e.g., $d = 1$ for single-step sampling), c) $v_\theta(l, 0, t, \mathbf{x}_t)$ with only length-wise shortcuts supports any ODE solver including more advanced ones with adaptive steps, and d) $v_\theta(l, d, t, \mathbf{x}_t)$ is the general setup with length- and time-wise shortcuts.

Conventional architectures that are implemented as neural networks $v_\theta(t, \mathbf{x}_t)$ treat the target vector field $u_t(\phi_t(\mathbf{x}))$ with the diffeomorphism $\phi_t(\mathbf{x})$ as a single expressive function. However, widely used neural networks have layered architectures, and, moreover, they are typically implemented as a sequence of blocks. With this observation, we propose to define (6) as the *outer* ODE_t w.r.t. time t , whereas $v_\theta(t, \mathbf{x}_t)$ itself can represent the solution to an *inner* ODE_l w.r.t. its length l .

We convert conventional ODE_t to the proposed $\text{ODE}_t (\text{ODE}_l)$ in several steps. First, we redefine $\phi_t(\mathbf{x})$ as a compositional function $\phi_t^L \circ \dots \circ \phi_t^i \circ \dots \circ \phi_t^1(\mathbf{x}) \rightarrow \phi_t(\mathbf{x})$ with L layers. Then, we introduce the length-dependent variable l that activates only the first l layers in the compositional function $\phi_t(\mathbf{x})$. In other words, the extended diffeomorphism is defined as $\phi : \{1, \dots, L\} \times [0, 1] \times \mathbb{R}^D \rightarrow \mathbb{R}^D$. This assumption is valid for recent transformer-based architectures e.g., the DiT [18].

Architectural modifications. In a second step, we rewire the neural network to output the ODE_l solution as follows. We introduce the residual connections \mathbf{r}_t^i that propagate latent vectors from layer to layer, and time- and length-dependent outputs of $v_\theta(l, t, \mathbf{x}_t)$ as shown in Fig. 3. The former represents the solution to the inner ODE_l for the selected length l from the $\{1, \dots, L\}$ range. Then, the inner ODE_l processing for the fixed-step Euler method at a time t can be expressed as

$$v_\theta(l, t, \mathbf{x}_t) := \sum_{i=1}^l v_\theta^i(l, t, \mathbf{r}_t^i), \text{ and } \mathbf{r}_t^i = \mathbf{r}_t^{i-1} + \Delta v_\theta^i(l, t, \mathbf{r}_t^{i-1}), \quad (7)$$

where \mathbf{r}_t^i is the i -th layer residual ($\mathbf{r}_t^0 = \mathbf{x}_t$) and $\Delta = 1/l$ is the step size in the Euler solver.

Effectively, our architectural extension (7) shortcuts the complexity of the model in a manner similar to [13] but in the length dimension. Then, this provides an additional knob to control the complexity-quality tradeoff of sampled data as shown in Fig. 4. For example, our method can combine both time- and length-wise shortcuts or any combination of them. Also, this provides additional unique properties: ODE_t is solver-agnostic and $\text{ODE}_{l < L}$ decreases both the latency and memory usage. Although we rely on the most simple Euler method in (7), other solvers can be explored for ODE_l .

Training with length-wise shortcuts. In a third step, we describe the training procedure with the shortcuts introduced in (7) and impose consistency objective on the outputs of the length-dependent neural network. Note that the CFM’s conditional probability path and the vector field $u_t(\mathbf{x}|\mathbf{z})$ from (4) have not been influenced by the change in the neural network $v_\theta(l, t, \mathbf{x}_t)$ and have the same trajectories in the time dimension. Then, we follow the consistency training methods [25, 13] and add an additional length-consistency (LC) term to the optimization objective. This term depends on the uniformly sampled pair (l, l_{LC}) from the range $\{L_{\min}, \dots, L\}$, where L_{\min} is the minimal shortcut

Algorithm 1 ODE_t (ODE_l) training with time- and length-wise shortcuts that are facilitated by the time-consistency (TC) and length-consistency (LC) objectives, respectively.

Input: $q(z), p_t(x|z), u_t(x|z)$ for CFM/DM, $\theta \leftarrow \theta_0$
while training **do**
 $t \sim \mathcal{U}(0, 1), z \sim q(z), x_t \sim p_t(x|z)$ \triangleright Sec. 3
 $(l, l_{LC}) \sim \mathcal{U}\{L_{\min}, L\}$ $\triangleright l$ shortcuts
 $d \sim 1/2^{\mathcal{U}\{1, \log_2 T\}}$ $\triangleright d$ shortcuts
 $v_{LC} \leftarrow v_\theta(l, 0, t, x_t)$ \triangleright length consistency
 $v_{TC} \leftarrow v_\theta(l, 2d, t, x_t)$ \triangleright time consistency
 $u_{LC} \leftarrow \text{sg}(v_\theta(l_{LC}, 0, t, x_t))$ \triangleright stop gradient
 $u_{TC} \leftarrow \text{sg}(v_\theta(l, d, t, x_t) + v_\theta(l, d, t + d, x_{t+d}))$
 $\tilde{v}_\theta(l, d, t, x_t) \leftarrow [v_\theta(l, 0, t, x_t), v_{LC}, v_{TC}/2]$
 $\tilde{u}_t(x|z) \leftarrow [u_t(x|z), u_{LC}, u_{TC}]$
 $\theta \leftarrow \text{Update}(\theta, \nabla_\theta \|\tilde{v}_\theta(l, d, t, x_t) - \tilde{u}_t(x|z)\|^2)$
end while

Algorithm 2 Our sampling with the dynamically selected time shortcuts d and network layers l for the outer ODE_t and the inner ODE_l, respectively.

Input: $q(x_0), \theta,$
 $l \leftarrow \{L_{\min}, \dots, L\},$
 $d \leftarrow \{0, 1, \dots, 1/T\}$
function ODEsolve_l(t, x_t)
 $r_t^0 = x_t$
for all $i \in \{1, \dots, l\}$ **do**
 $r_t^i \leftarrow r_t^{i-1} + v_\theta^i(l, d, t, r_t^{i-1})$
end for
end function \triangleright return $v_\theta(l, d, t, x_t)$
 $t \leftarrow 0, x_t \sim q(x_0)$
 $x_1 \leftarrow \text{ODEsolve}_t \text{ODEsolve}_l(t, x_t)$
return x_1

length. Formally, our length-consistent training objective is defined as

$$\arg \min_{\theta} \mathcal{L} := \mathbb{E}_{(l, l_{LC}) \sim \mathcal{U}\{L_{\min}, L\}} [\|v_\theta(l, t, x_t) - u_t(x|z)\|^2 + \|v_\theta(l, t, x_t) - \text{sg}(v_\theta(l_{LC}, t, x_t))\|^2], \quad (8)$$

where sg is the stop-gradient operator, and $t \sim \mathcal{U}(0, 1), x_t \sim p_t(x|z)$ are from Section 3.

Enforcing the self-consistency by bootstrapping the neural network targets in the (8) second term has shown its efficiency in [49, 13]. This reduces the variance in the first empirical term and, instead, replaces it with deterministic neural network targets in the second term. To avoid a major increase in training time when calculating these targets, the mini-batch with the (8) loss is constructed to contain only a small portion (e.g., $K = 1/8$) of the deterministic consistency terms, while the rest of it contains empirical CFM terms. In general, our method extends the time-wise shortcuts from [13] which is outlined in Algorithms 1-2 with the summary of all proposed steps.

Additional details. We introduce two learnable embeddings for, correspondingly, length l and time d shortcuts as presented in Algs. 1-2. The outputs of these embeddings are added to the conventional positional and classifier-free label embeddings. Then, their overall representation is used to condition each block as in [18]. In other words, our length embedding is the only additional module compared to [13] which results in an insignificant additional computational overhead.

We also experiment with a modification in which blocks can be combined into groups. Then, each group contains G blocks and represents a single Euler step in ODE_l. For example, a sequence of L blocks with $G = 1$ is equivalent to (8). When $G = 2$, the number of available length-wise shortcuts is halved i.e. $L/2$. The conventional architecture without the inner ODE_l is equivalent to the $G = L$ option. Therefore, we can empirically verify how our ODE_l approach affects the sampling performance metrics by varying the group hyperparameter $G \in \{1, \dots, L\}$.

5 Experiments

This section explores the quality-complexity tradeoff for various corner cases that have been enabled by our approach as illustrated in Fig. 4. Also, we investigate this tradeoff from the fixed- vs. adaptive-step ODE solver perspective, and perform ablation studies: finding the optimal group size G and the hyperparameter K for the introduced length-consistency objective. We compare ODE_t (ODE_l)-derived models with prior distillation and shortcut methods using performance vs. computational complexity metrics. Our code is JAX-based with ODE solvers from the *diffraX* library [50].

5.1 Experimental setup

Datasets and evaluation. We experiment with CelebA-HQ [51] for unconditional generation and ImageNet [52] for class-conditional generation. We use 256×256 image resolution in all experiments. After training, we sample images using Euler fixed-step solver with 1, 4, and 128 time steps T in the

outer ODE_T following [13] experiments. We also use the classifier-free guidance [53] in ImageNet sampling when $T = 128$ and define the latter as total number of inference passes. Additionally, we employ Dormand-Prince’s 5/4 (Dopri5) adaptive-step solver [54] without time discretization to highlight that our method is solver-agnostic and to show the practical feasibility of such solvers.

The quality of the generated images is evaluated using the Fréchet inception distance (FID) metric [55]. We report the FID-50K metric that is measured for 50,000 sampled images w.r.t. the corresponding dataset statistics. The metric is estimated using 2048-length latent activations by running the InceptionV3 neural network with public weights [56]. Before processing activations, generated images are resized to 299×299 resolution with bilinear interpolation and clipped to the $[-1, 1]$ range.

Architectures and baselines. By default, we follow Frans et al. [13] setup and employ the DiT-B [18] architecture which consists of a sequence with 12 transformer blocks in our experiments. Additionally, we investigate scaling laws using the DiT-XL with a sequence of 28 blocks and larger latent-space dimensions in the Appendix A. Importantly, the DiT architecture itself operates in the latent space of the pretrained variational autoencoder (VAE) (i.e. *sd-vae-ft-mse*) from Rombach et al. [57] with $8\times$ downscaling and upscaling in the encoder and decoder spatial resolutions, respectively.

We use the improved DiT-based variance preserving diffusion model [58] from [18] and the same model but trained using the rectified flow matching (RFM) objective [3] from Table 1 as *baselines without any compute optimizations*. Then, we report reference results for distillation methods from Section 2 that have been reimplemented by Frans et al. [13] for the RFM model. Distillation methods include *two-stage methods* with teacher-student training such as progressive distillation [21] and Reflow from [3], and *single-stage* or *end-to-end methods* without student i.e. the consistency training [24], live Reflow as well as time-wise shortcut model (SM) from [13].

We extend the SM code³ by adopting it to a recent JAX version for GPU experiments and by modifying the bootstrapping from fixed to uniformly sampled targets with the support of arbitrary batch sizes. Then, we experiment with the revised SM implementation and our ODE_t (ODE_l)-derived RFM models as follows. We start from the public SM checkpoint to save training time in larger-scale ImageNet experiments, while we initialize all models from scratch in CelebA-HQ experiments. Next, we train baselines and ODE_t (ODE_l) variants for 200,000 iterations using the schedule and hyperparameters from Table 7. We report the FID-50K metric as $\mu \pm \sigma$ where the mean μ and standard deviation error bars $\pm \sigma$ have been estimated using 4 runs with different seeds.

For the sake of brevity, we mark our runs by the type of train-time ODE: a) ODE_t for continuous-time RFM, b) ODE_T for discrete-time RFM ($T = 128$), and c) $\text{ODE}_{T|d}$ for discrete-time SM with conditioning on shortcuts d . This notation is further extended to all our ODE_t (ODE_l) setups. For example, $\text{ODE}_{T|l,d}(\text{ODE}_{l=8})$ denotes the proposed method with length- and time-wise shortcuts where the neural network contains only 8 of the 12 active blocks for DiT-B.

5.2 Quantitative results

Table 2 presents the image generation results for CelebA-HQ-256 and ImageNet-256 datasets using the standard FID-50K metric. In particular, images have been sampled using the fixed-step Euler solver with T time steps. Note that the upper part contains reference results from Frans et al. [13] which can diverge with ours due to differences in library versions, training hyperparameters and hardware. The bottom part shows our experimental results including: three baselines and our models with length- and time-wise shortcuts (i.e., $\text{ODE}_{T|l,d}(\text{ODE}_{l \in \{4,8,12\}})$). Our results in Table 2 are mostly in line with the reference runs, and our model further decreases complexity by shortcutting the DiT-B from 12 blocks to 8 blocks with only a minor drop in quality of sampled CelebA-HQ images. When combined with time-wise shortcuts, our $\text{ODE}_{T|l,d}(\text{ODE}_{l=4,8})$ configurations can further improve the quality-complexity tradeoff as also illustrated in Fig. 2 with latency scaling. On the other hand, ImageNet results show lower compute-per-FID savings due to large data distribution and class-conditional sampling that have been increased with a larger DiT-XL network in Appendix A.

Next, we study whether the common fixed-step Euler solver is optimal for all corner cases in Table 3. We measure actual wall-clock time (WCT) latency to sample a mini-batch of images (excluding the VAE processing) for the Euler solver with T time steps and adaptive-step Dopri5 solver with the reported tolerance (tol.) levels. We highlight that in our method both the WCT latency and the

³github.com/kvfrans/shortcut-models/

Table 2: **Image generation quality scaling for prior work and our ODE_t (ODE_l)-derived models.** Image quality is estimated using the FID-50K metric (lower is better) using the DiT-B architecture for CelebA-HQ-256 and ImageNet-256 datasets. Compute is proportional to the number of time steps in the Euler method, $T \in \{1, 4, 128\}$. In our method, compute and memory also decrease with the neural network length, $l \in \{4, 8, 12\}$. Hence, our ODE_t (ODE_l) encompasses both directions.

Dataset	Train. stages	CelebA-HQ-256 (uncond.)			ImageNet-256 (class-cond.)		
Time steps, $T = 1/d$		128	4	1	128	4	1
reference results from [13]:							
DM [18]	1	23.0	(123)	(132)	39.7	(465)	(467)
RFM[3] (ODE_T):	1	7.3	63.3	(281)	17.3	(108)	(325)
+ Progres. dist. [21]	2	(303)	(251)	14.8	(202)	(143)	35.6
+ Reflow [3]	2	16.1	18.4	23.2	16.9	32.8	44.8
+ Consist. train. [24]	1	53.7	19.0	33.2	42.8	43.0	69.7
+ Live Reflow [13]	1	6.3	27.2	43.3	46.3	95.8	58.1
+ SM ($\text{ODE}_{T d}$) [13]	1	<u>6.9</u>	13.8	<u>20.5</u>	15.5	28.3	<u>40.3</u>
our experimental results:							
RFM (ODE_t)	1	6.1	63.2	(286)	-	-	-
RFM (ODE_T):	1	6.1	65.6	(287)	-	-	-
+SM ($\text{ODE}_{T d}$)	1	<u>6.0</u>	19.2	24.1	<u>15.0</u>	<u>17.7</u>	<u>36.2</u>
+ $\text{ODE}_{T l,d}(\text{ODE}_{l=12})$	1	5.9± 0.1	19.6 ± 0.3	25.3 ± 0.3	14.8± 0.1	15.4± 0.1	20.3± 0.3
+ $\text{ODE}_{T l,d}(\text{ODE}_{l=8})$	1	7.9 ± 0.1	19.4 ± 0.3	24.3 ± 0.3	23.0 ± 0.2	24.4 ± 0.3	36.6 ± 0.8
+ $\text{ODE}_{T l,d}(\text{ODE}_{l=4})$	1	14.2 ± 0.1	19.5 ± 0.1	31.0 ± 0.2	64.2 ± 0.4	64.6 ± 0.5	95.3 ± 1.0

Table 3: **Fixed- vs. adaptive-step solvers.** We compare FID, memory usage (MEM), and wall-clock time (WCT) to sample 128-size mini-batch using DiT-B for CelebA-HQ-256, sec. When our solver-agnostic method is used with Dopri5 and certain tolerance (tol.), results show that adaptive-step solvers are a better choice for high-quality sampling with low latency and memory usage.

Euler/Dopri5	MEM \downarrow	T/tol	FID \downarrow	WCT \downarrow	T/tol	FID \downarrow	WCT \downarrow
SM ($\text{ODE}_{T d}$)	1 \times	128	6.0	12.9	4	19.2	0.40
$\text{ODE}_{T l,d}(\text{ODE}_{l=12})$	1 \times	128	5.9	13.0	4	19.6	0.41
$\text{ODE}_{t l}(\text{ODE}_{l=12})$	1 \times	1e-4	5.9	7.3	1e-2	6.1	3.49
$\text{ODE}_{T l,d}(\text{ODE}_{l=8})$	0.67 \times	128	7.9	8.7	4	19.4	0.27
$\text{ODE}_{t l}(\text{ODE}_{l=8})$	0.67 \times	1e-4	7.1	4.9	1e-2	7.3	2.25
$\text{ODE}_{T l,d}(\text{ODE}_{l=4})$	0.33 \times	128	14.2	4.3	4	19.5	0.14
$\text{ODE}_{t l}(\text{ODE}_{l=4})$	0.33 \times	1e-4	13.8	2.4	1e-2	14.5	1.14

memory usage are linear with the neural network length and there is a minor latency overhead for the additional length embedder (e.g., 0.4 seconds for SM vs. 0.41 for ours with $l = 12$). Table 3 shows that Dopri5 can sample images with high quality (lower FID) and significantly lower latency. For example, the SM method achieves 6.0 FID in 12.9 seconds, while our $\text{ODE}_{t|l}(\text{ODE}_{l=8})$ with Dopri5 and 1e-4 tolerance reaches 5.9 FID in only 7.3 seconds, or with 1e-2 tolerance 7.3 FID in 2.3 seconds. Hence, *adaptive-step solvers are a better choice in the high-quality sampling regime, while fixed-step solvers are only optimal for a few step low-quality generation* as shown in Fig. 2 scaling curves.

5.3 Ablation study and qualitative results

We perform ablation studies for key hyperparameters that accompany the framework proposed in Section 4 using the CelebA-HQ dataset. First, we vary the group size constant G that defines how many steps are performed in the inner ODE_l and, hence, the number of options for the neural network length. As expected, Table 4 results show that the larger groups with higher expressivity lead to better (lower) FID scores. Surprisingly, it is not the case when l and T are high and $G = 1$. This can be related to better gradient propagation during training with more residual connections.

Table 4: **Ablation study: group size.** Larger group sizes lead to better (lower) FID metrics when l and T are low, but result in less choices for dynamic neural network length l selection.

Euler steps, T	128	4	1
$l = 8, G = 1$	7.4	20.3	26.2
$l = 8, G = 2$	<u>7.8</u>	19.3	<u>26.1</u>
$l = 8, G = 4$	7.9	<u>19.4</u>	24.3
$l = 4, G = 1$	18.1	21.5	36.9
$l = 4, G = 2$	<u>16.2</u>	<u>20.9</u>	<u>35.4</u>
$l = 4, G = 4$	14.2	19.5	31.0

Table 5: **Ablation study: length-consistency.** Higher consistency regularization hyperparameter K helps to improve FID in the most compute-efficient configurations i.e. when l and T are low.

Euler steps, T	128	4	1
$l = 8, K = 0$	7.6	19.5	24.4
$l = 8, K = 1/8$	<u>7.9</u>	<u>19.4</u>	<u>24.3</u>
$l = 8, K = 1/4$	8.2	19.1	23.7
$l = 4, K = 0$	14.8	19.5	31.6
$l = 4, K = 1/8$	<u>14.2</u>	19.5	<u>31.0</u>
$l = 4, K = 1/4$	14.0	19.5	30.1

Second, we investigate the hyperparameter K that defines the share of length-consistency terms within mini-batches during training. According to Table 5 study, our length-consistency is important in the most compute-optimized modes i.e. when l and T are low. We hypothesize that it regularizes how much a teacher with more blocks forces a shorter-length student to mimic its vector field output.

Our representative sampling results for CelebA-HQ are shown in Fig. 1 using the 3×3 image grid. We decrease generation time steps T horizontally from 128 to only a single step, and the length l vertically from the full 12 blocks to only 4 blocks. The upper row is equivalent to time-wise shortcuts [13], where we can see noticeable changes in the image style caused by the time-consistency objective. On the other hand, our length-wise shortcuts with the length-consistency objective (8) preserve the style and iteratively compress the image details. The bottom right corner combines both approaches with artifacts of two kinds and the benefit of extremely fast sampling ($92\times$ lower latency w.r.t. the top left corner). We provide more CelebA-HQ qualitative examples in the Appendix C as well as examples generated by DiT-B and the larger DiT-XL architecture for ImageNet dataset.

6 Discussion

In this paper, we presented the ODE_t (ODE_l) that incorporates the shortcuts in the neural network length dimension. Effectively, it generalizes the recent class of knowledge distillation methods i.e. the time-wise shortcut models for even faster ODE-based sampling from flow and diffusion models.

Our generalization involved few architecture-level modifications and a new consistency training objective with minimal computational overhead. Moreover, the proposed method also includes additional unique features, such as solver-agnostic ODE_t and the reduction of memory usage when $\text{ODE}_{l < L}$. Image generation experiments for CelebA-HQ and ImageNet have shown further improvement in the quality-complexity tradeoff scaling including the feasibility study of adaptive-step solvers.

Limitations. The ODE_l presumes an architecture that consists of a sequence with directly connected blocks. Although this is easily applicable to recent transformer-based architectures, it is less trivial to apply our modifications to backbones with hierarchical multiscale feature aggregation, as in U-Nets [59]. The latter require additional changes e.g., implementation of scale-wise shortcuts.

Future work. Relaxing the integration order in ODEs and adding other features can lead to additional benefits e.g., generation with iteratively increasing data quality without recomputations when leveraging each available length-wise shortcut. Another interesting direction for very large models is the research on early exit strategies, where the quality-complexity tradeoff can be estimated and the decision to shortcut can be made at sampling time with low computational overhead.

Broader impact. We introduced a method to increase the sampling speed at lower computational cost for diffusion and flow models. These models are widely used in many applications that range from image generation for the general public to discovery of new materials and healthcare drugs. Therefore, this work can lead to acceleration of the results in these fields and to overall energy savings.

References

- [1] Yaron Lipman, Ricky T. Q. Chen, Heli Ben-Hamu, Maximilian Nickel, and Matthew Le. Flow matching for generative modeling. In *ICLR*, 2023.
- [2] Michael Samuel Albergo and Eric Vanden-Eijnden. Building normalizing flows with stochastic interpolants. In *ICLR*, 2023.
- [3] Xingchao Liu, Chengyue Gong, and Qiang Liu. Flow straight and fast: Learning to generate and transfer data with rectified flow. In *ICLR*, 2023.
- [4] Jascha Sohl-Dickstein, Eric A. Weiss, Niru Maheswaranathan, and Surya Ganguli. Deep unsupervised learning using nonequilibrium thermodynamics. In *ICML*, 2015.
- [5] Yang Song and Stefano Ermon. Generative modeling by estimating gradients of the data distribution. In *NeurIPS*, 2019.
- [6] Jonathan Ho, Ajay Jain, and Pieter Abbeel. Denoising diffusion probabilistic models. In *NeurIPS*, 2020.
- [7] Patrick Esser, Sumith Kulal, Andreas Blattmann, Rahim Entezari, Jonas Müller, Harry Saini, Yam Levi, Dominik Lorenz, Axel Sauer, Frederic Boesel, Dustin Podell, Tim Dockhorn, Zion English, and Robin Rombach. Scaling rectified flow transformers for high-resolution image synthesis. In *ICML*, 2024.
- [8] Omer Bar-Tal, Hila Chefer, Omer Tov, Charles Herrmann, Roni Paiss, Shiran Zada, Ariel Ephrat, Junhwa Hur, Guanghui Liu, Amit Raj, et al. Lumiere: A space-time diffusion model for video generation. In *SIGGRAPH Asia*, 2024.
- [9] Subham Sekhar Sahoo, Marianne Arriola, Aaron Gokaslan, Edgar Mariano Marroquin, Alexander M Rush, Yair Schiff, Justin T Chiu, and Volodymyr Kuleshov. Simple and effective masked diffusion language models. In *NeurIPS*, 2024.
- [10] Tomas Geffner, Kieran Didi, Zuobai Zhang, Danny Reidenbach, Zhonglin Cao, Jason Yim, Mario Geiger, Christian Dallago, Emine Kucukbenli, Arash Vahdat, and Karsten Kreis. Proteina: Scaling flow-based protein structure generative models. In *ICLR*, 2025.
- [11] Hongyu Guo, Yoshua Bengio, and Shengchao Liu. AssembleFlow: Rigid flow matching with inertial frames for molecular assembly. In *ICLR*, 2025.
- [12] Shufan Li, Konstantinos Kallidromitis, Akash Gokul, Zichun Liao, Yusuke Kato, Kazuki Kozuka, and Aditya Grover. OmniFlow: Any-to-any generation with multi-modal rectified flows. In *CVPR*, 2025.
- [13] Kevin Frans, Danijar Hafner, Sergey Levine, and Pieter Abbeel. One step diffusion via shortcut models. In *ICLR*, 2025.
- [14] Alexander Tong, Kilian Fatras, Nikolay Malkin, Guillaume Hugué, Yanlei Zhang, Jarrid Rector-Brooks, Guy Wolf, and Yoshua Bengio. Improving and generalizing flow-based generative models with minibatch optimal transport. *Transactions on Machine Learning Research*, 2024.
- [15] Yang Song, Jascha Sohl-Dickstein, Diederik P Kingma, Abhishek Kumar, Stefano Ermon, and Ben Poole. Score-based generative modeling through stochastic differential equations. In *ICLR*, 2021.
- [16] Xuhui Fan, Zhangkai Wu, and Hongyu Wu. A survey on pre-trained diffusion model distillations. *arXiv:2502.08364*, 2025.
- [17] Sander Dieleman. The paradox of diffusion distillation, 2024. URL <https://sander.ai/2024/02/28/paradox.html>.
- [18] William Peebles and Saining Xie. Scalable diffusion models with transformers. In *ICCV*, 2023.
- [19] Geoffrey Hinton, Oriol Vinyals, and Jeff Dean. Distilling the knowledge in a neural network. *arXiv:1503.02531*, 2015.

- [20] Eric Luhman and Troy Luhman. Knowledge distillation in iterative generative models for improved sampling speed. *arXiv:2101.02388*, 2021.
- [21] Tim Salimans and Jonathan Ho. Progressive distillation for fast sampling of diffusion models. In *ICLR*, 2022.
- [22] Chenlin Meng, Robin Rombach, Ruiqi Gao, Diederik Kingma, Stefano Ermon, Jonathan Ho, and Tim Salimans. On distillation of guided diffusion models. In *CVPR*, 2023.
- [23] Yuanzhi Zhu, Xingchao Liu, and Qiang Liu. SlimFlow: Training smaller one-step diffusion models with rectified flow. In *ECCV*, 2025.
- [24] Yang Song, Prafulla Dhariwal, Mark Chen, and Ilya Sutskever. Consistency models. In *ICML*, 2023.
- [25] Yang Song and Prafulla Dhariwal. Improved techniques for training consistency models. In *ICLR*, 2024.
- [26] Zhengyang Geng, Ashwini Pokle, Weijian Luo, Justin Lin, and J Zico Kolter. Consistency models made easy. In *ICLR*, 2025.
- [27] Simian Luo, Yiqin Tan, Longbo Huang, Jian Li, and Hang Zhao. Latent consistency models: Synthesizing high-resolution images with few-step inference. *arXiv:2310.04378*, 2023.
- [28] Qiang Liu. Rectified flow: A marginal preserving approach to optimal transport. *arXiv:2209.14577*, 2022.
- [29] Emmanuel Bengio, Pierre-Luc Bacon, Joelle Pineau, and Doina Precup. Conditional computation in neural networks for faster models. In *ICLR*, 2016.
- [30] Zuxuan Wu, Tushar Nagarajan, Abhishek Kumar, Steven Rennie, Larry S. Davis, Kristen Grauman, and Rogerio Feris. BlockDrop: Dynamic inference paths in residual networks. In *CVPR*, 2018.
- [31] Xin Wang, Fisher Yu, Zi-Yi Dou, Trevor Darrell, and Joseph E. Gonzalez. SkipNet: Learning dynamic routing in convolutional networks. In *ECCV*, 2018.
- [32] Tal Schuster, Adam Fisch, Tommi Jaakkola, and Regina Barzilay. Consistent accelerated inference via confident adaptive transformers. In Marie-Francine Moens, Xuanjing Huang, Lucia Specia, and Scott Wen-tau Yih, editors, *Proceedings of the Conference on Empirical Methods in Natural Language Processing*, 2021.
- [33] Tae Hong Moon, Moonseok Choi, EungGu Yun, Jongmin Yoon, Gayoung Lee, Jaewoong Cho, and Juho Lee. A simple early exiting framework for accelerated sampling in diffusion models. In *ICML*, 2024.
- [34] Wangbo Zhao, Yizeng Han, Jiasheng Tang, Kai Wang, Yibing Song, Gao Huang, Fan Wang, and Yang You. Dynamic diffusion transformer. In *ICLR*, 2025.
- [35] Haoran You, Connelly Barnes, Yuqian Zhou, Yan Kang, Zhenbang Du, Wei Zhou, Lingzhi Zhang, Yotam Nitzan, Xiaoyang Liu, Zhe Lin, Eli Shechtman, Sohrab Amirghodsi, and Yingyan Celine Lin. Layer-and timestep-adaptive differentiable token compression ratios for efficient diffusion transformers. In *CVPR*, 2025.
- [36] Xingjian Bai and Luke Melas-Kyriazi. Fixed point diffusion models. In *CVPR*, 2024.
- [37] Shaojie Bai, J Zico Kolter, and Vladlen Koltun. Deep equilibrium models. In *NeurIPS*, 2019.
- [38] Zhengyang Geng and J. Zico Kolter. Torchdeq: A library for deep equilibrium models. <https://github.com/locuslab/torchdeq>, 2023.
- [39] Yiping Lu, Aoxiao Zhong, Quanzheng Li, and Bin Dong. Beyond finite layer neural networks: Bridging deep architectures and numerical differential equations. In *ICML*, 2018.

- [40] Amir Gholami, Kurt Keutzer, and George Biros. ANODE: Unconditionally accurate memory-efficient gradients for neural ODEs. In *IJCAI*, 2019.
- [41] Junyu Zhang, Daochang Liu, Eunbyung Park, Shichao Zhang, and Chang Xu. Residual learning in diffusion models. In *CVPR*, 2024.
- [42] Marin Biloš, Johanna Sommer, Syama Sundar Rangapuram, Tim Januschowski, and Stephan Günnemann. Neural flows: Efficient alternative to neural ODEs. In *NeurIPS*, 2021.
- [43] Zhiyuan Ma, Liangliang Zhao, Biqing Qi, and Bowen Zhou. Neural residual diffusion models for deep scalable vision generation. In *NeurIPS*, 2024.
- [44] Zichao Long, Yiping Lu, Xianzhong Ma, and Bin Dong. PDE-net: Learning PDEs from data. In *ICML*, 2018.
- [45] Ricky T. Q. Chen, Yulia Rubanova, Jesse Bettencourt, and David K Duvenaud. Neural ordinary differential equations. In *NeurIPS*, 2018.
- [46] Will Grathwohl, Ricky T. Q. Chen, Jesse Bettencourt, and David Duvenaud. Scalable reversible generative models with free-form continuous dynamics. In *ICLR*, 2019.
- [47] Juntang Zhuang, Nicha Dvornek, Xiaoxiao Li, Sekhar Tatikonda, Xenophon Papademetris, and James Duncan. Adaptive checkpoint adjoint method for gradient estimation in neural ODE. In *ICML*, 2020.
- [48] Qinsheng Zhang and Yongxin Chen. Fast sampling of diffusion models with exponential integrator. In *ICLR*, 2023.
- [49] Jiatao Gu, Shuangfei Zhai, Yizhe Zhang, Lingjie Liu, and Joshua M. Susskind. BOOT: Data-free distillation of denoising diffusion models with bootstrapping. In *ICML 2023 Workshop on Structured Probabilistic Inference & Generative Modeling*, 2023.
- [50] Patrick Kidger. *On Neural Differential Equations*. PhD thesis, University of Oxford, 2021.
- [51] Tero Karras, Timo Aila, Samuli Laine, and Jaakko Lehtinen. Progressive growing of GANs for improved quality, stability, and variation. In *ICLR*, 2018.
- [52] J. Deng, W. Dong, R. Socher, L.-J. Li, K. Li, and L. Fei-Fei. ImageNet: A Large-Scale Hierarchical Image Database. In *CVPR*, 2009.
- [53] Jonathan Ho and Tim Salimans. Classifier-free diffusion guidance. In *NeurIPS 2021 Workshop on Deep Generative Models and Downstream Applications*, 2021.
- [54] J. R. Dormand and P. J. Prince. A family of embedded Runge–Kutta formulae. *J. Comp. Appl. Math*, 6:19–26, 1980.
- [55] Martin Heusel, Hubert Ramsauer, Thomas Unterthiner, Bernhard Nessler, and Sepp Hochreiter. GANs trained by a two time-scale update rule converge to a local nash equilibrium. In *NeurIPS*, 2017.
- [56] Matthias Wright. FID computation in JAX/Flax, 2021. URL <https://github.com/matthias-wright/jax-fid/>.
- [57] Robin Rombach, Andreas Blattmann, Dominik Lorenz, Patrick Esser, and Björn Ommer. High-resolution image synthesis with latent diffusion models. In *CVPR*, 2022.
- [58] Alexander Quinn Nichol and Prafulla Dhariwal. Improved denoising diffusion probabilistic models. In *ICML*, 2021.
- [59] Olaf Ronneberger, Philipp Fischer, and Thomas Brox. U-Net: Convolutional networks for biomedical image segmentation. In Nassir Navab, Joachim Hornegger, William M. Wells, and Alejandro F. Frangi, editors, *Medical Image Computing and Computer-Assisted Intervention (MICCAI)*, 2015.
- [60] Prafulla Dhariwal and Alexander Quinn Nichol. Diffusion models beat GANs on image synthesis. In *NeurIPS*, 2021.

A ImageNet-256 experiments with DiT-XL

In Table 6 (top), we provide a comparison to recent diffusion models on ImageNet-256 dataset with a large NFE budget T . In Table 6 (bottom), we also report results with the DiT-XL network for the time-wise shortcut model (SM) [13] and ODE_t (ODE_l) including the SM reference results and our experimental results with variable NFE budget $T \in \{128, 4, 1\}$. We finetune our model using approximately 43 epochs (200,000 iterations with batch size of 256 as specified in Table 7) from the SM public checkpoint to avoid a very long training with 250 epochs. Table 6 (bottom) shows that ODE_t (ODE_l) scales well compared to the SM baseline. For example, memory and/or latency can be reduced with a minor drop in FID when the length l is selected to be 20 out of 28 DiT-XL blocks.

Table 6: **ImageNet-256 experiments with DiT-XL and comparison to recent diffusion models.**

Model	FID	T time steps			Param. count	Train. epochs		
DiT-XL [18]	2.3	500			675M	640		
ADM-G [60]	4.6	250			554M	426		
LDM-4-G [57]	3.6	500			400M	106		
T time steps	FID	FID-50K			Latency, sec			Train. epochs
		128	4	1	128	4	1	
ref. SM DiT-XL [13]	3.8	7.8	10.6					250
ours SM DiT-XL [13]	4.1	7.9	9.4		32.0	1.1	0.4	43
$\text{ODE}_{T l,d}(\text{ODE}_{l=28})$	5.3	7.5	11.9		32.1	1.1	0.4	43
$\text{ODE}_{T l,d}(\text{ODE}_{l=20})$	7.5	16.1	34.4		21.3	0.7	0.3	43
$\text{ODE}_{T l,d}(\text{ODE}_{l=12})$	11.9	32.5	69.4		10.7	0.3	0.2	43

Table 7: **Implementation details and hyperparameters.**

Dataset	CelebA-HQ-256		ImageNet-256
Architecture	DiT-B	DiT-B	DiT-XL
Patch size	2×2	2×2	2×2
Hidden size	768	768	1152
Attention heads	12	12	16
MLP hidden ratio	4	4	4
Blocks $\{L_{\min}, L\}$	$\{4, 12\}$	$\{4, 12\}$	$\{12, 28\}$
Default G, K	$4, 1/8$	$4, 1/8$	$8, 1/8$
Training iterations	$100K \rightarrow 100K$		
Learning rate	$1e-4 \rightarrow 1e-5$		
Batch size	128	256	256
Initial weights	from scratch	from [13] checkpoint	
Schedule	90% const. with 5,000 iter. warmup \rightarrow 10% cosine decay		
Optimizer	AdamW with $\beta_1 = 0.9, \beta_2 = 0.999$ and weight decay = 0.1		
EMA ratio	0.999		
Class. free guid.	0	1.5	1.5
GPUs	$4 \times \text{A6000}$	$8 \times \text{A6000}$	$8 \times \text{H100}$
Generation	uncond.	class-cond.	class-cond.
Classes	1	1000	1000
ODE _l solver	Euler by the neural network		
ODE _t solver	Euler/Dopri5	Euler	Euler
EMA weights	✓	✓	✓

B Implementation details

We report the implementation details in Table 7. Typical DiT-B training run with 200,000 iterations takes 2 days using A6000 GPUs, while DiT-XL training takes 1 day using H100 GPUs.

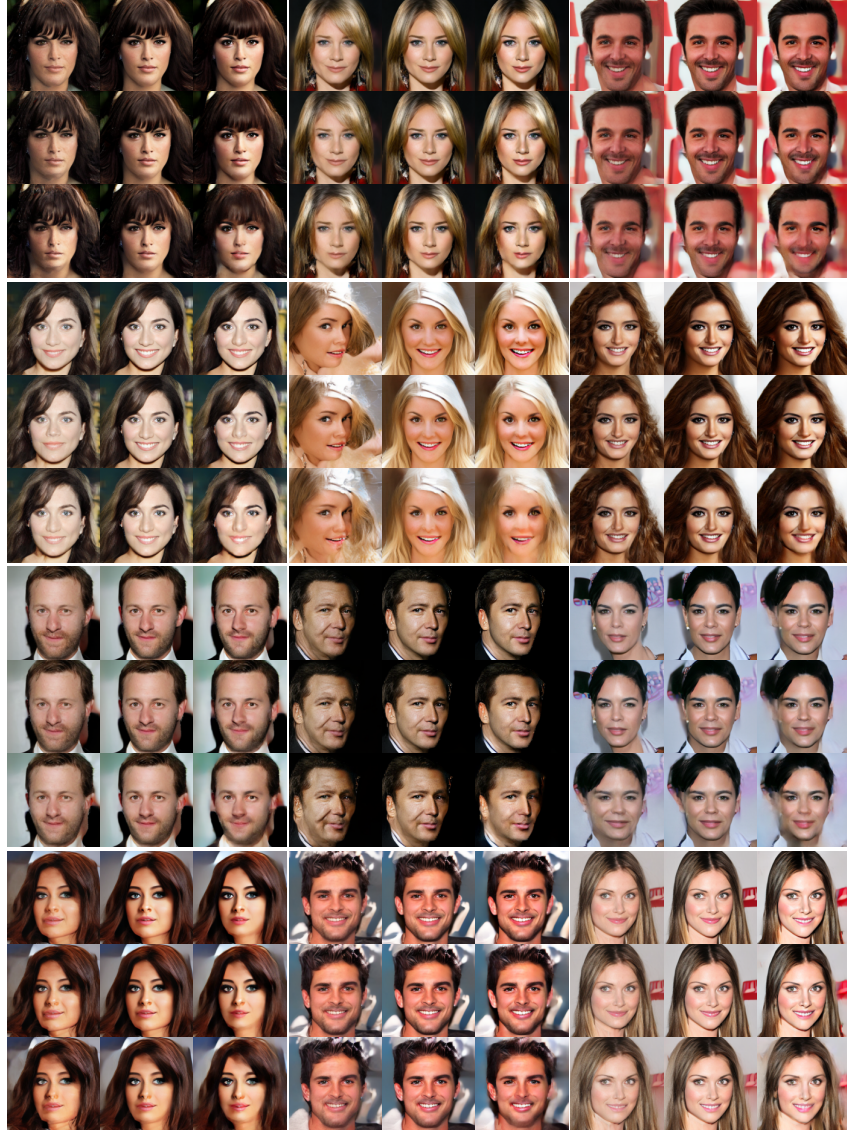


Figure 5: CelebA-HQ-256 images generated by $\text{ODE}_{T|l,d}(\text{ODE}_l)$ with DiT-B. Time shortcuts [13] (columns with $T = 128, 4, 1$ from left to right) alter the image style, our length-wise shortcuts (rows $l = 12, 8, 4$ from top to bottom) preserve the style and iteratively compress the image details.

C Qualitative results

Our additional qualitative sampling results for CelebA-HQ and ImageNet-1K with DiT-B/XL architectures are shown in Figures 5-6 using the same 3×3 image grids. The generation time steps $T = 128, 4, 1$ decrease horizontally from left to right. The neural network length decreases vertically from top to bottom with $l = 12, 8, 4$ for DiT-B and $l = 28, 20, 12$ for DiT-XL, respectively. The upper row is equivalent to time-wise shortcuts [13], where we can see noticeable changes in the image style caused by the time-consistency objective. On the other hand, our length-wise shortcuts with the length-consistency objective preserve the style and iteratively compress the image details. The bottom right corner combines both approaches with artifacts of two types and the benefit of extremely fast sampling with a factor of $100\times$ lower latency w.r.t. the top left corner.

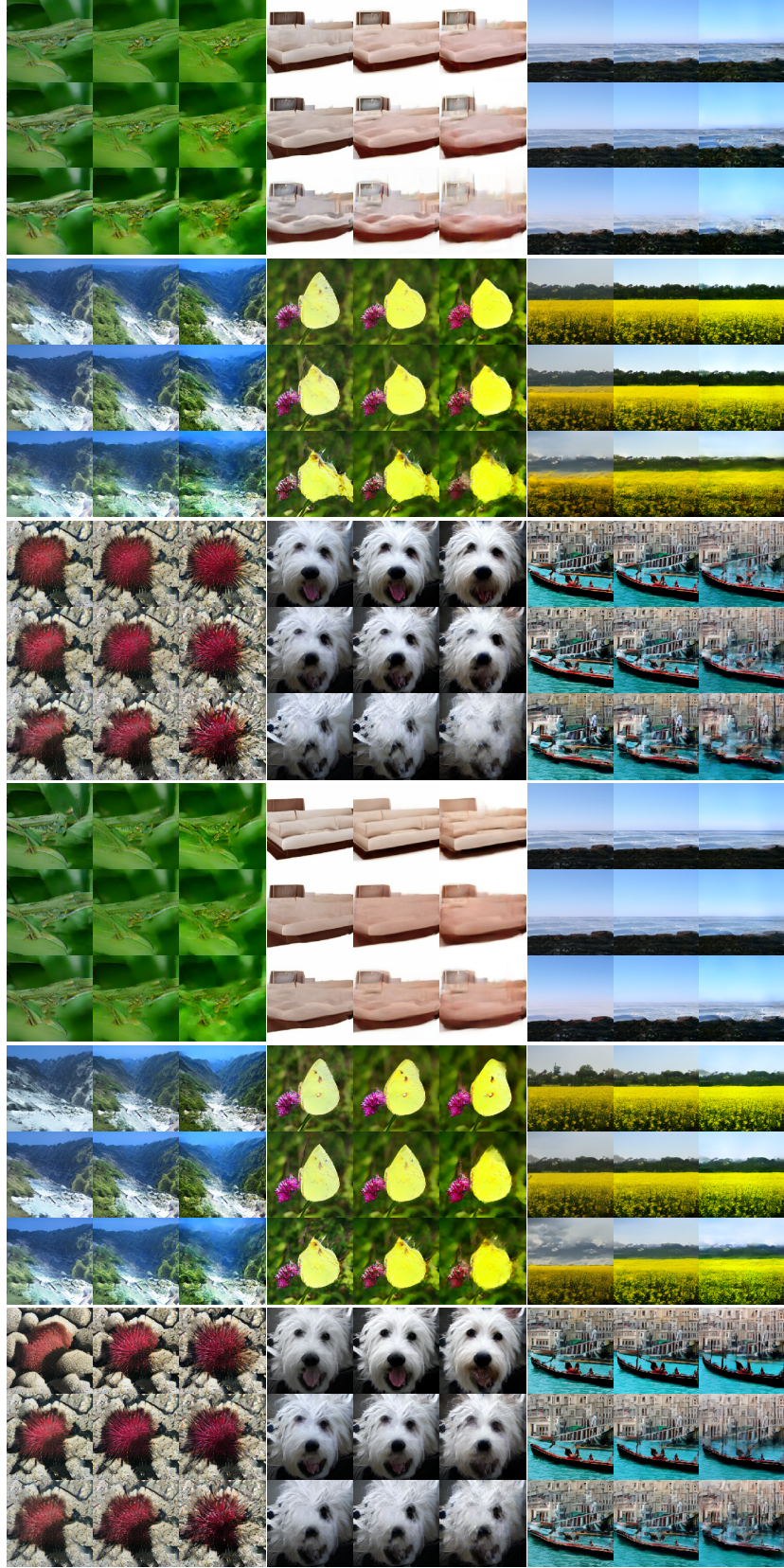


Figure 6: ImageNet-256 images generated by $ODE_{T|l,d}(ODE_l)$ with DiT-B (top) and DiT-XL (bottom). Time shortcuts [13] (column-wise from left to right) alter the image style, our length-wise shortcuts (row-wise from top to bottom) preserve the style and iteratively compress the image details.